applied optics

Evanescent coupling between refillable ring resonators and laser-inscribed optical waveguides

Hengky Chandrahalim,[1,2] Stephen C. Rand,[2] and Xudong Fan[2,*]

[1]Department of Biomedical Engineering, University of Michigan, Ann Arbor, Michigan 48109, USA
[2]Department of Electrical Engineering and Computer Science, University of Michigan, Ann Arbor, Michigan 48109, USA
*Corresponding author: xsfan@umich.edu

Received 22 March 2017; revised 10 May 2017; accepted 12 May 2017; posted 12 May 2017 (Doc. ID 290947); published 30 May 2017

We investigated theoretically and experimentally the evanescent coupling between photonic waveguides of arbitrary shapes and refillable optical ring resonators on the same chip. The resonator hosts were designed to facilitate whispering gallery modes and etched by using a single-mask standard lithography process, whereas the waveguides were imprinted in the proximity of the ring resonator by using 3D ultrafast laser-writing technology. Finite element analysis in conjunction with coupled-mode theory revealed a coupling Q-factor (Q_C) of approximately 10^6. The polymer core ring resonator exhibited a loaded Q-factor (Q_T) as high as 5.4×10^4 and a free spectral range (FSR) of 406 pm at a center wavelength of 775 nm. Long-term stability of the ring resonator was repeatedly tested by examining the spectral location of optical resonances and the constancy of Q-factors and FSRs under ambient laboratory conditions for 1 month. We recorded consistent Q-factors and repeatable FSRs for all measurements. Renewability of the polymer core was demonstrated by removing and redepositing the polymer in the cavity, followed by measurements of Q-factors and FSRs. This work promises to enable reconfigurable and renewable photonic devices for on-chip lasers, 3D integrated optical signal processing, chip-scale molecular sensing, and the investigation of new optical phenomena.

OCIS codes: (130.0130) Integrated optics; (230.5750) Resonators; (140.3948) Microcavity devices; (230.7370) Waveguides.

https://doi.org/10.1364/AO.56.004750

1. INTRODUCTION

Transparent dielectric cavities that support whispering gallery modes (WGMs) are attractive because of their capability to trap streams of photons in small optical mode volumes for a long time. This enhances the circulating intensity of light and generates a wide range of applications, such as biosensing [1,2], nanoparticle sizing [3], single molecule detection [4], optical signal processing [5,6], and on-chip microlasers [7–9]. In addition, the high-quality factors (Q-factors) of WGM microcavities can result in optical intensities high enough to excite various kinds of nonlinear phenomena [10,11]. Although off-chip WGM microresonators with Q-factors $\sim 10^{10}$ have been previously demonstrated [12], many practical applications demand chip-scale sustainable microresonators that have integrated optical waveguides to reliably couple light into and out of the cavity.

Microring and microdisk WGM optical cavities still retain their respectable Q-factors even when they are fabricated on a chip [13–16]. They have a simple form factor, small size, and the ability to support a broad range of wavelengths. High Q-factor polymer ring resonators with integrated waveguides have been fabricated on robust substrates with lithographic nanoimprinting [17]. However, the fabrication of such resonators requires expensive electron-beam (e-beam) lithography to pattern the mold and additional treatments to smoothen it. Moreover, the exposed gaps between the waveguides and ring structures are prone to contamination, and the entire nanoimprinting process must be repeated once the device fails. Recently, we developed highly versatile microring resonators with straightforward, rapid, and economical fabrication processes to provide optical feedback in microlaser systems [7–9]. Furthermore, our successful attempt in employing ultrafast laser pulses to inscribe optical waveguides on the same die [9] suggests that it is practical to use the same hybrid fabrication method to combine passive microring resonators and waveguides on a single fused-silica chip.

Here we report the theoretical analysis and successful experimental demonstration of evanescent light coupling between optical waveguides inscribed by a femtosecond laser and photolithographically fabricated refillable microring resonators. The ring resonator is an exposed trench that can accept any solid or liquid transparent dielectric materials whose refractive indices are higher than that of fused-silica. The embedded waveguide is used to couple the coherent light into and out of the ring cavity. The laser-writing process exploits a nonlinear light-matter interaction that locally induces a refractive index increase

(core-cladding index difference of $\sim 5.25 \times 10^{-3}$) [18] and is capable of creating arbitrary 3D geometries to guide light into the optical resonator and transport the output light from the resonators to any direction within the fused-silica substrate. Unlike previously demonstrated integrated ring resonator-waveguide systems [19–21], the photonic waveguides presented here are simple, low-cost, and can be rapidly and accurately patterned with a single-step maskless ultrafast laser-writing process at room temperature and standard atmospheric pressure. They are well protected within the surrounding fused-silica, yet physically connected to the high-index material deposited in the ring cavity host through the solid low-index fused-silica gap. This integrated structure enables a passive refillable resonator system with excellent robustness, durability, broad chemical compatibility, and good thermal stability. Finite element analysis (FEA) in conjunction with the coupled-mode theory was employed to analyze the coupling efficiency between microring cavity and waveguide and revealed a coupling Q-factor (Q_C) of approximately 10^6. The polymer core ring resonator was characterized and exhibited a loaded Q-factor (Q_T) as high as 5.4×10^4 and free spectral range (FSR) of 406 pm at a center wavelength of 775 nm. Long-term stability of the ring resonator was tested by monitoring the optical resonances and FSRs under standard laboratory conditions for over 1 month. We recorded reproducible Q-factors and FSRs in all measurements. Renewability of the polymer core

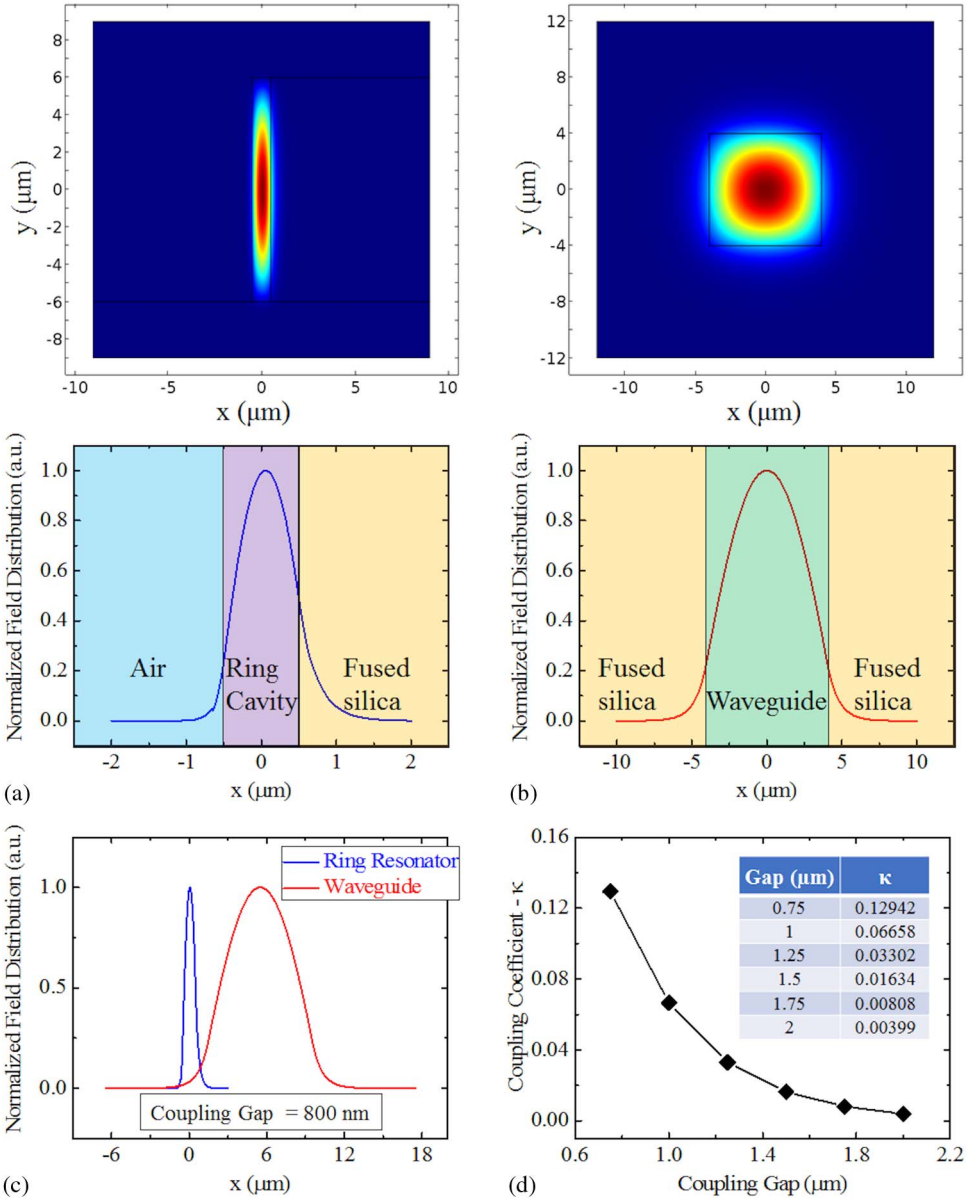

Fig. 1. (a) FEA of the fundamental optical mode in the polymer ring resonator, where color represents the electric field of the optical mode (top figure) and normalized field distribution along the thickness of the ring resonator at $y = 0$ (bottom figure); (b) FEA of the fundamental optical mode in the refractive index modified optical waveguide, where color represents the electric field of the optical mode (top figure) and normalized field distribution along the width of the waveguide at $y = 0$ (bottom figure); (c) overlap of evanescent fields in the ring resonator and waveguide for an 800 nm coupling gap; (d) plot of coupling coefficient (κ) between the ring resonator and optical waveguide as a function of the coupling gap.

was demonstrated by depositing, removing, and redepositing SU-8 polymer on the ring cavity host, followed by measurements of Q-factors and FSRs.

2. THEORETICAL MODELING

We started the integrated photonic system design by theoretically estimating the coupling efficiency between the ring resonator and waveguide using FEA followed by coupled-mode theory [22,23]. The finite element mode analysis was performed on a cross section in the xy plane of the ring resonator and waveguide. The wave propagates in the z direction and has the form of $\tilde{E}(x, y, z, t) = \tilde{E}(x, y)e^{j(\omega t-\beta z)}$, where ω, t, and β are the angular frequency, time, and propagation constant, respectively. The fundamental optical mode distribution in the xy plane of the ring resonator and optical waveguide are presented in Figs. 1(a) and 1(b) (top figures). We then computed the evanescent fields in the ring resonator and waveguide at $y = 0$. The results are plotted in Figs. 1(a) and 1(b) (bottom figures). We estimated the coupling efficiency of our waveguide to the polymer ring resonator according to the formula [23]

$$\kappa^2 = \left[\frac{2\pi R}{\gamma}e^{\left(-\frac{(\Delta\beta)^2 R}{\gamma}\right)}\right]\frac{k^4}{4\beta_{\mathrm{RR}}\beta_{\mathrm{WG}}}(n_{\mathrm{WG}}^2 - n_{\mathrm{FS}}^2)(n_{\mathrm{RR}}^2 - n_{\mathrm{FS}}^2) \times \int_{\mathrm{WG}} e_{\mathrm{WG}}e_{\mathrm{RR}}\,\mathrm{d}x \int_{\mathrm{RR}} e_{\mathrm{WG}}e_{\mathrm{RR}}\,\mathrm{d}x. \quad (1)$$

The subscripts RR, WG, and FS refer to the ring resonator, waveguide, and the fused-silica substrate, respectively. The evanescent electric field distributions in the waveguide and ring resonator are described by e_{WG} and e_{RR}, respectively, and both fields are normalized to their respective total intensity in the xy plane. All parameters that we used to estimate the coupling efficiency between the waveguide and the ring resonator are tabulated in Table 1. The overlap of evanescent fields in the ring resonator and waveguide for an 800 nm coupling gap is shown in Fig. 1(c). We computed their overlap integral for different coupling gaps and estimated the coupling coefficient (κ). The values of κ as a function of various coupling gaps are plotted in Fig. 1(d). The coupling coefficient, κ of our current device was approximately 0.11, which corresponds to a Q_C of $\sim 10^6$ when use is made of the relation $Q_C = kn_{\mathrm{RR}}L/\kappa^2$.

Table 1. Parameters Used to Analyze the Coupling Efficiency between the Optical Waveguide and Polymer Ring Resonator

Parameter	Definition	Value	Unit
λ	Wavelength of operation	780	nm
R	Ring radius	150	μm
L	Length of the cavity	$2\pi R$	μm
γ	Decay constant of RR	5.658	μm^{-1}
β_{RR}	Propagation constant of the RR	11.9	μm^{-1}
β_{WG}	Propagation constant of the WG	11.76	μm^{-1}
$\Delta\beta$	$\beta_{\mathrm{RR}} - \beta_{\mathrm{WG}}$	0.14	μm^{-1}
k	$2\pi/\lambda$	8.06	μm^{-1}
n_{RR}	Refractive index of RR	1.62	–
n_{WG}	Refractive index of WG	1.465	–
n_{FS}	Refractive index of FS	1.460	–
e_{RR}	Guided mode decay in RR	–	–
e_{WG}	Guided mode decay in WG	–	–
κ	Coupling coefficient	Plotted in Fig. 1(d)	–

3. DESIGN AND FABRICATION

The ring resonator host structure was designed to have inner and outer radii and depth of 110, 150, and 12 μm, respectively. It was fabricated with a wafer-level single-mask bulk micromachining process as outlined in Fig. 2(a). A 100 mm diameter fused-silica wafer was spin-coated with a 16 μm thick negative-tone photoresist and soft-baked. A contact aligner was used to expose the wafer to UV light. The wafer was then developed with a tetramethylammonium hydroxide (TMAH)-based photoresist developer (Step 1). A reactive ion glass etcher was used to etch the fused-silica wafer. Our fused-silica etching recipe has been characterized to consistently provide the sidewall roughness of better than 30 nm (Step 2). After the etching process, the wafer was diced into 1 cm × 1 cm chips with a dicing saw.

The optical waveguide inscription process was performed with ultrashort laser pulses (wavelength $\lambda = 800$ nm, pulse width 100 fs, pulse energy 0.3 μJ, and repetition rate 250 kHz) focused with a 50× objective into the diced fused-silica chip (Step 3). The laser spot diameter on the sample was approximately 1 μm. Multiple-pass laser writing in 3D was executed to form an optical waveguide with cross-sectional dimensions of 8 μm × 8 μm. The scanning speed of the substrate varied from 0.05 to 2 mm/s, depending on the local geometry of the ring cavities. The femtosecond laser pulse energy and repetition rate were carefully optimized during the waveguide inscription to prevent crack formation along the inner wall of the ring cavity. Our current waveguide writing technology has allowed for inscriptions of optical waveguides ~800 nm away from the sidewalls of a patterned bulk-fused silica without causing any damages to the sidewalls. Detailed waveguide writing parameters have been previously presented elsewhere [18]. The loss of such inscribed optical waveguides in fused silica is consistently measured to be less than 0.15 dB/cm at 1550 nm. We measured the optical powers at the input and output ports of the waveguide at 780 nm wavelength and recorded a total loss of lower than 0.4 dB/cm. Once the ring resonator host and waveguide are integrated, transparent dielectrics can be conveniently deposited onto and removed from the fused-silica chip (Step 4). We spin-coated the polymer using a photoresist spinner and measured its thickness by using a surface profilometer. We targeted to have a 1 μm thick of polymer layer on the sidewall of the ring resonator host, with variations of within +/ – 40 nm. Due to the mechanical and chemical robustness of the device, the above procedures can be repeated indefinitely. The scanning electron microscope (SEM) image in Fig. 2(b) shows that the ring resonator host was crack-free, although the waveguide was written only 800 nm away from the outer wall of the ring. Since the photo-induced refractive index change is less than 1% of the nominal refractive index of fused silica, the inscribed waveguide is not visible under bright field microscope imaging. However, it is evident under a differential interference contrast (DIC) microscope [Fig. 2(c)]. Guidance and confinement of the microscope illumination light from the cross-sectional perspective of the waveguide at the edge of the chip is presented in Fig. 2(d).

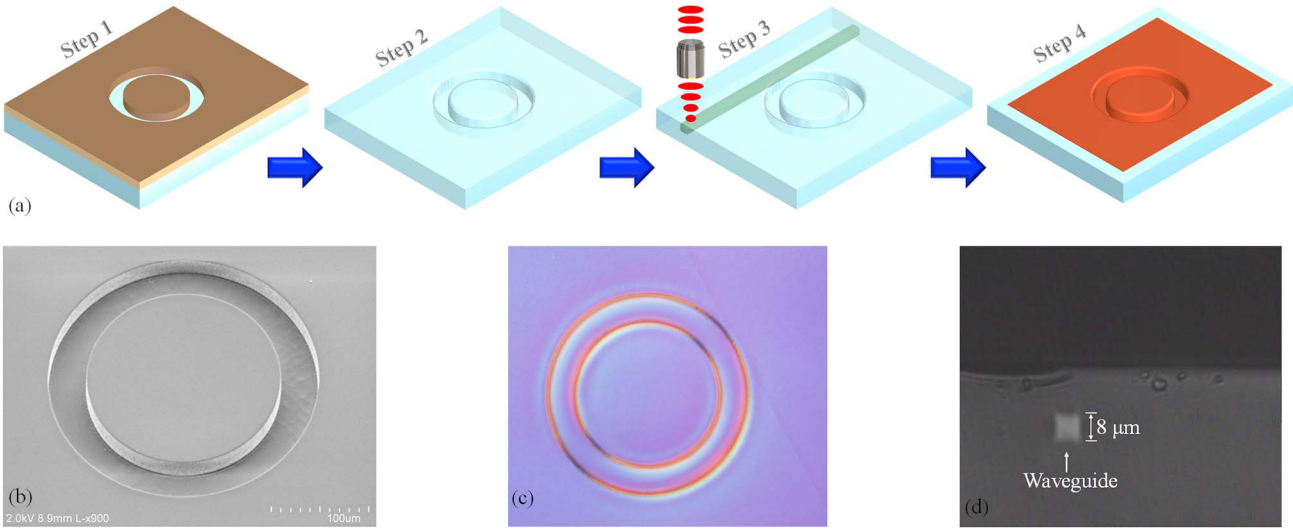

Fig. 2. (a) Fabrication process flow of the ring resonators: 16 μm thick KMPR negative-tone photoresist was spin-coated and patterned on the top of the fused-silica wafer. Next, the fused-silica wafer was anisotropically etched by using a reactive-ion etcher. The optical waveguide was then inscribed 800 nm away from the ring resonator by using femtosecond laser pulses. Finally, 1 μm thick layer of high refractive index polymer was deposited and cured on the surface of the cavity; (b) SEM image of the fabricated ring resonator exhibiting smooth and crack-free inner-wall of the ring cavity around the vicinity where the optical waveguide was inscribed by femtosecond laser pulses; (c) DIC microscope image of the same ring resonator revealing the refractive index modified optical waveguide inscribed by a femtosecond laser next to the resonator; (d) cross-sectional view of the waveguide at the edge of the chip, demonstrating distinct guidance and confinement of the microscope illumination light.

4. EXPERIMENTAL

We characterized the device according to the measurement setup outlined in Fig. 3. The input light was transmitted to the optical polarization controller and then butt-coupled into the on-chip waveguide from a narrow linewidth, continuous-wave (CW) tunable laser centered at 775 nm via a single-mode optical fiber, whereas the output light was captured by a multimode fiber and subsequently detected by an optical power meter. The input fiber tip, device under test (DUT), and collection fiber tip were mounted on threeaxis micropositioning stages with independent controls (not shown in Fig. 3). Two cameras were used simultaneously to precisely couple the input light from the fiber to the on-chip waveguide and the output light from the on-chip waveguide to the collection fiber. Optical resonances, observed as dips in transmitted output intensity, were acquired by a computer that concurrently controlled the CW laser and power meter.

After initial alignment, we performed a series of experiments under standard laboratory conditions for the entire period of 1 month to examine the long-term stability of our integrated

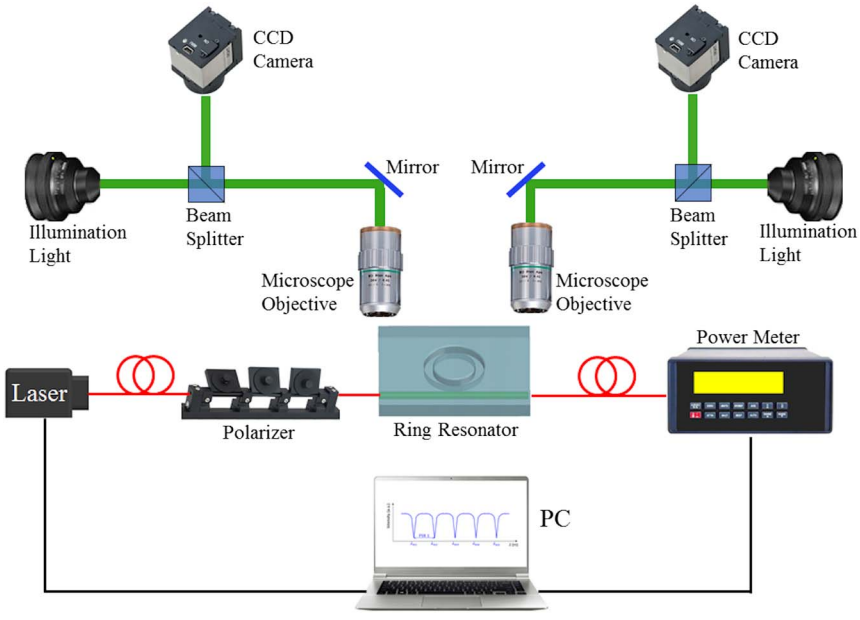

Fig. 3. Schematic of the measurement setup.

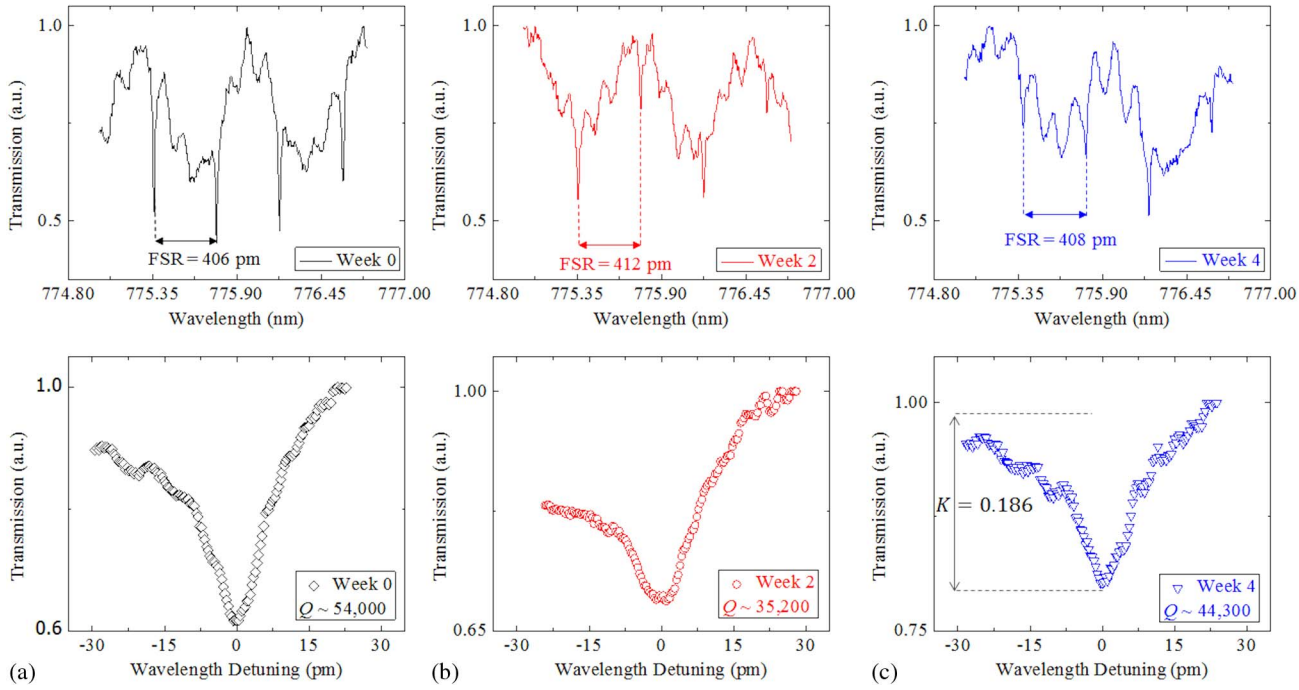

Fig. 4. Series of measurements to verify the long-term stability of the ring resonator: measurement taken (a) immediately, (b) 2 weeks, and (c) 4 weeks after the deposition of high refractive index polymer on the ring resonator (top graphs: coarse scan measurements and bottom graphs: fine scan measurements).

ring-waveguide system. The DC motor in the tunable laser source was first controlled to sweep a wide range of wavelength (over 4 × theoretical FSR). When the wavelength matched the resonant condition of the WGM in the ring resonator, the output power dropped, allowing the WGM spectral locations to be identified as shown in the top graphs of Fig. 4. We recorded relatively consistent FSR values of 406–412 pm during all these experiments. These experimentally measured FSR values are only about 0.7–1.5% higher than the theoretically calculated FSR of 403 pm, obtained from the relation $\mathrm{FSR} = \lambda^2/(2\pi R n_{\mathrm{RR}})$, where $\lambda = 780$ nm, $R = 150$ μm, and $n_{\mathrm{RR}} = 1.62$. In addition to the WGM resonances, we also observed distinct oscillations in the background of all wide-scan measurements with periods of oscillations fluctuating between 150 and 700 pm. Similar FSR analyses were done, and we concluded that these background oscillations resulted from Fabry–Perot cavity effects that were formed between the input and output fibers and the corresponding edges of the fused-silica chip. Refractive index-matching materials can be used to solve this issue in future experiments. In order to characterize loaded Q-factors of the device, we conducted fine wavelength sweeps over 60 pm. The loaded Q-factors, Q_T, varied from 35,000 to 55,000 for optical resonances with center wavelengths of 775.364 nm [Fig. 4(a) (bottom)], 775.358 nm [Fig. 4(b) (bottom)], and 775.387 nm [Fig. 4(c) (bottom)] over a period of 1 month.

The coupling efficiency between the ring resonator and optical waveguide is characterized by the fractional depth K, which describes the fraction of energy extracted into the ring resonator from the waveguide [22,23]. K is related to κ through $K = 4Q_C Q_0/(Q_C + Q_0)^2$, where Q_0 is the intrinsic Q-factor of the ring resonator and $Q_C = k n_{\mathrm{RR}} L/\kappa^2$. The coupling condition is known as under-coupled if $Q_0 < Q_C (K < 1)$, critically coupled if $Q_0 = Q_C (K = 1)$, or overcoupled if $Q_0 > Q_C (K > 1)$. The Q_C of our device was estimated by FEA in conjunction with coupled-mode theory to be $\sim 10^6$. Considering our measured data in Fig. 4(c), we achieved a Q_T of 44,300. Subsequently, we deduced a value of $Q_0 = 46,503$ through the relation $1/Q_T = 1/Q_C + 1/Q_0$. K can then be computed from the known values of Q_C and Q_0 as 0.181. This value matches the measured K value of 0.186 closely, as indicated in Fig. 4(c).

One of the major advantages of our ring resonator platform over other existing on-chip resonator technologies is that its core material can be renewed or reconfigured, which is easily accomplished by removing and redepositing different types and phases of transparent dielectric materials in the cavity host. For example, it was simple to remove the old polymer from the chip using Remover PG solution and subsequently deposit a new polymer. In order to justify the renewability of our ring resonator, we removed the old polymer from the chip, redeposited a new polymer, and performed the customary characterization steps and obtained the results presented in Fig. 5. The center wavelength of the newly deposited polymer ring resonator was observed to be 775.259 nm. We also achieved FSR and Q-factor similar to our previous experiments.

5. CONCLUSION

In conclusion, we have demonstrated theoretically and experimentally the evanescent coupling between a refillable, open-channel, microring resonator with highly flexible ultrafast

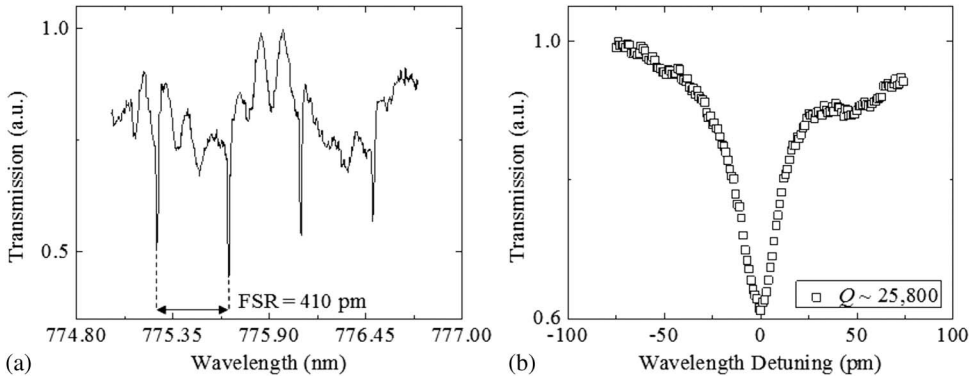

Fig. 5. Consistent resonances were recorded from the same ring resonator host after removal and re-depositions of high refractive index polymer (a) coarse measurement and (b) fine measurement.

laser-imprinted photonic waveguides on the same chip. The uniquely integrated optical resonator system presented here offers competitive benefits compared to other chip-scale optical resonators. It has a wide range of operational wavelengths and incorporates embedded waveguides that offer great degrees of freedom. Additionally, the system is inexpensive and easy to assemble, which allows for rapid prototyping. It has inherent mechanical robustness and durability for repeated use. The transparent dielectric materials that confine WGM in the cavity host can be extended to fluidic phase materials, thereby extending the applicability of these structures to the flourishing field of optofluidics. The order of the ring-resonator can be scaled up to realize coupled-resonator systems in 3D to facilitate ultra-high density on-chip photonic signal processors. Hybrid integration technology of this caliber will enable the investigation of novel nonlinear phenomena at low input power levels, such as parity-time (PT) symmetry and nonreciprocity in nonlinear optics [24,25], as well as molecular magnetoelectric effects on photonic chips [26–28].

Funding. National Science Foundation (NSF) (ECCS-1303499, ECCS-1607250, DBI-1451127); Air Force Office of Scientific Research (AFOSR) (AFOSR FA9550_12_1_0119).

Acknowledgment. The authors thank Translume Inc. for inscribing the optical waveguides.

REFERENCES

1. X. Fan, I. M. White, S. I. Shopova, H. Zhu, J. D. Suter, and Y. Sun, "Sensitive optical biosensors for unlabeled targets: a review," Anal. Chim. Acta **620**, 8–26 (2008).
2. H. K. Hunt and A. M. Armani, "Label-free biological and chemical sensors," Nanoscale **2**, 1544–1559 (2010).
3. J. Zhu, S. K. Ozdemir, Y.-F. Xiao, L. Li, L. He, D.-R. Chen, and L. Yang, "On-chip single nanoparticle detection and sizing by mode splitting in an ultrahigh-Q microresonator," Nat. Photonics **4**, 46–49 (2010).
4. F. Vollmer and S. Arnold, "Whispering-gallery-mode biosensing: label-free detection down to single molecules," Nat. Methods **5**, 591–596 (2008).
5. V. R. Almeida, C. A. Barrios, R. R. Panepucci, and M. Lipson, "All-optical control of light on a silicon chip," Nature **431**, 1081–1084 (2004).
6. B. Little, S. Chu, P. Absil, J. Hryniewicz, F. Johnson, F. Seiferth, D. Gill, V. Van, O. King, and M. Trakalo, "Very high-order microring resonator filters for WDM applications," IEEE Photon. Technol. Lett. **16**, 2263–2265 (2004).
7. H. Chandrahalim, Q. Chen, A. A. Said, M. Dugan, and X. Fan, "Monolithic optofluidic ring resonator lasers created by femtosecond laser nanofabrication," Lab Chip **15**, 2335–2340 (2015).
8. H. Chandrahalim and X. Fan, "Reconfigurable solid-state dye-doped polymer ring resonator lasers," Sci. Rep. **5**, 18310 (2015).
9. H. Chandrahalim, S. C. Rand, and X. Fan, "Fusion of renewable ring resonator lasers and ultrafast laser inscribed photonic waveguides," Sci. Rep. **6**, 32668 (2016).
10. V. S. Ilchenko, A. A. Savchenkov, A. B. Matsko, and L. Maleki, "Nonlinear optics and crystalline whispering gallery mode cavities," Phys. Rev. Lett. **92**, 043903 (2004).
11. T. J. Kippenberg, R. Holzwarth, and S. Diddams, "Microresonator-based optical frequency combs," Science **332**, 555–559 (2011).
12. W. Liang, A. A. Savchenkov, Z. Xie, J. F. McMillan, J. Burkhart, V. S. Ilchenko, C. W. Wong, A. B. Matsko, and L. Maleki, "Miniature multioctave light source based on a monolithic microcavity," Optica **2**, 40–47 (2015).
13. P. De Heyn, D. Vermeulen, D. Van Thourhout, and G. Roelkens, "Silicon-on-insulator all-pass microring resonators using a polarization rotating coupling section," IEEE Photon. Technol. Lett. **24**, 1176–1178 (2012).
14. A. Griffith, J. Cardenas, C. B. Poitras, and M. Lipson, "High quality factor and high confinement silicon resonators using etchless process," Opt. Express **20**, 21341–21345 (2012).
15. B. Momeni, S. Yegnanarayanan, M. Soltani, A. A. Eftekhar, E. S. Hosseini, and A. Adibi, "Silicon nanophotonic devices for integrated sensing," J. Nanophoton. **3**, 031001 (2009).
16. B. J. Hausmann, I. Bulu, P. Deotare, M. McCutcheon, V. Venkataraman, M. Markham, D. Twitchen, and M. Loncar, "Integrated high-quality factor optical resonators in diamond," Nano Lett. **13**, 1898–1902 (2013).
17. T. Ling, S.-L. Chen, and L. J. Guo, "High-sensitivity and wide-directivity ultrasound detection using high Q polymer microring resonators," Appl. Phys. Lett. **98**, 204103 (2011).
18. Y. Bellouard, A. Said, and P. Bado, "Integrating optics and micromechanics in a single substrate: a step toward monolithic integration in fused silica," Opt. Express **13**, 6635–6644 (2005).
19. Z. Li, "Optofluidic coupled micro-ring resonators for biosensing," in *IEEE International Frequency Control Symposium (FCS)* (IEEE, 2012), pp. 1–4.
20. G. Testa, C. Collini, L. Lorenzelli, and R. Bernini, "Planar silicon-polydimethylsiloxane optofluidic ring resonator sensors," IEEE Photon. Technol. Lett. **28**, 155–158 (2016).
21. G. Testa, Y. Huang, P. M. Sarro, L. Zeni, and R. Bernini, "Integrated silicon optofluidic ring resonator," Appl. Phys. Lett. **97**, 131110 (2010).
22. M. L. Gorodetsky and V. S. Ilchenko, "Optical microsphere resonators: optimal coupling to high-Q whispering-gallery modes," J. Opt. Soc. Am. B **16**, 147–154 (1999).

23. I. M. White, H. Oveys, X. Fan, T. L. Smith, and J. Zhang, "Integrated multiplexed biosensors based on liquid core optical ring resonators and antiresonant reflecting optical waveguides," Appl. Phys. Lett. **89**, 191106 (2006).
24. B. Peng, Ş. Özdemir, S. Rotter, H. Yilmaz, M. Liertzer, F. Monifi, C. Bender, F. Nori, and L. Yang, "Loss-induced suppression and revival of lasing," Science **346**, 328–332 (2014).
25. B. Peng, Ş. K. Özdemir, F. Lei, F. Monifi, M. Gianfreda, G. L. Long, S. Fan, F. Nori, C. M. Bender, and L. Yang, "Parity-time-symmetric whispering-gallery microcavities," Nat. Phys. **10**, 394–398 (2014).
26. S. C. Rand, W. Fisher, and S. L. Oliveira, "Optically induced magnetization in homogeneous, undoped dielectric media," J. Opt. Soc. Am. B **25**, 1106–1117 (2008).
27. A. A. Fisher, E. F. C. Dreyer, A. Chakrabarty, and S. C. Rand, "Optical magnetization, part I: experiments on radiant optical magnetization in solids," Opt. Express **24**, 26055–26063 (2016).
28. A. A. Fisher, E. F. C. Dreyer, A. Chakrabarty, and S. C. Rand, "Optical magnetization, part II: theory of induced optical magnetism," Opt. Express **24**, 26064–26079 (2016).